this reason, Eq. (22) is rewritten in the form

$$\sigma = C_\sigma \Gamma^{-N} e n^{1/2} / m^{1/2} \tag{24}$$

Since $N=3/2$ for the $T=0$ metal, it is to be expected that $N>0$ for the completely degenerate electron plasma, i.e., its conductivity decreases with increasing nonideality Γ[Eq. (24)]. This formula is useful for the interpretation of conductivity data of completely degenerate electron plasmas, with N as the adjustable parameter.

In a partially degenerate electron plasma, $E_T \lesssim E_Q$, the conductivity depends on the dimensional parameters e, m, n, KT, and $\hbar$. By Eq. (3),

$$\sigma = C_\sigma e^{N_1} m^{N_2} n^{N_3} (KT)^{N_4} \hbar^{N_5} \tag{25}$$

Comparison of the powers of $\mathfrak{L}$, $\mathfrak{M}$, and $\mathfrak{T}$ in Eq. (25) gives three independent equations, which permit to express three of the five powers in terms of the remaining ones,

$$N_1 = 1 - 2A - 2B, \qquad N_2 = -\frac{1}{2} - B$$

$$N_3 = \frac{1}{2} - \frac{1}{3}A + \frac{1}{3}B, \qquad N_4 \equiv A, \quad N_5 \equiv 2B \tag{26}$$

Hence, the conductivity of the $T>0$ quantum plasma is

$$\sigma = C_\sigma \left(\frac{KT}{e^2 n^{1/3}}\right)^A \left(\frac{\hbar^2 n^{1/3}}{me^2}\right)^B e n^{1/2} / m^{1/2} \tag{27}$$

where A and B are powers which cannot be determined by dimensional reasoning.

For $A=-1$ and $B=-3/2$, Eq. (27) yields the conductivity of solid metals at temperatures $T>0$,

$$\sigma = C_\sigma \frac{me^6}{\hbar^3} \frac{n^{1/3}}{KT}, \quad A=-1, \quad B=-3/2 \tag{28}$$

where[17] $C_\sigma \propto Z^{-1/3}$. Equation (28) expresses the $1/T$ law[17] of the metallic conductivity at "high temperatures."

Equation (27) contains the dimensionless groups γ and Γ, which permit rewriting the conductivity formula as

$$\sigma = C_\sigma \gamma^{-A} \Gamma^{-B} e n^{1/2} / m^{1/2} \tag{29}$$

Since $A=-1$ for $T>0$ metals [Eq. (28)] and $B=3/2$ for $T=0$ metals [Eq. (23)], one can speculate that $A \gtrsim -1$ and $B>0$ for nonideal, partially degenerate plasmas. A and B can readily be determined by means of conductivity measurements for nonideal quantum plasmas.

The dimensionless coefficient C_σ can be determined experimentally or by calculation of the momentum exchange of the electrons from a kinetic equation for nonideal classical and quantum plasmas, respectively. For ideal and weakly nonideal plasmas, $0 \leq \gamma \ll 1$, the coefficient C_σ varies very little[12] with n and T. For proper nonideal plasmas, C_σ is a true constant when many particle interactions are dominant. For these reasons, the coefficient C_σ is of secondary importance concerning the dependence of the conductivity σ on the variables n and T.

Conclusion

We have derived new conductivity formulas for nonideal classical $T>0$ plasmas [Eq. (17) or (19)], completely degenerate plasmas [Eqs. (22) and (23)], and nonideal $T>0$ quantum plasmas [Eqs. (27) and (28)]. These formulas can be used to interprete conductivity measurements on nonideal plasmas. Once the still undetermined powers N, A, and B are known empirically, it should be possible to develop a conductivity theory for nonideal plasmas that provides an explanation of the γ and Γ dependence from microscopic principles.

Acknowledgment

This work was supported by the U. S. Office of Naval Research.

References

[1] Franck, E. U., and Hensel, F., "Metallic Conductance of Supercritical Mercury Gas at High Pressure," *Physical Review*, Vol. 147, 1966, pp. 109-110.

[2] Renkert, H., Hensel, F., and Franck, E. U., "Metal-Nonmetal Transition in Dense Cesium Vapor," *Physics Letters*, Vol. 30A, 1969, pp. 494-495.

[3] Barolskii, S. H., Ermokhin, N. V., Kulik, P. P., and Melnikov, V. M., "Measurement of Electric Conductivity of Dense Strongly Nonideal Cesium Plasma," *Soviet Physics, Journal of Experimental and Theoretical Physics*, Vol. 35, 1976, pp. 94-97.

[4] Ivanov, Yu. V., Mintsev, V. B., Fortov, V. E., and Dremin, A. N., "Electric Conductivity of Nonideal Plasma," *Soviet Physics, Journal of Experimental and Theoretical Physics*, Vol. 44, 1976, pp. 112-116.

[5] Goldbach, C., Nollez, G., Popovic, S., and Popovic, M., "Electric Conductivity of High Pressure Ionized Argon," *Zeitschrift fuer Naturforschung*, Vol. 33a, 1977, pp. 11-16.

[6] Ermokhin, N. V., Kovalec, B. M., Kulik, P. P., and Ryabyi, V. A., "Temperature Dependence of Electric Conduction of Dense Cesium Plasma," *Journal de Physique*, Vol. 39, Supp. 5, 1978, pp. 200-204.

[7] Wilhelm, H. E., "Momentum and Energy Exchange Between Beams of Particles Interacting by Yukawa Type Potentials," *Physical Review*, Vol. 187, 1969, pp. 382-392.

[8] Alekseev, V. A., "Measurement of Electric Conductivity and Density of Metals in the Supercritical State," *High Temperature*, Vol. 8, 1970, pp. 597-611.

[9] Ermokhin, N. V., Kovalev, B. M., Kulik, P. P., and Ryabyi, V. A., "An Experimental Investigation of Coulomb Interactions in Dense Plasmas," *High Temperature*, Vol. 9, 1971, pp. 611-618.

[10] Lomakin, B. N. and Fortov, V. E., "Equation of State of Nonideal Cesium Plasma," *Soviet Physics, Journal of Theoretical and Experimental Physics*, Vol. 36, 1973, pp. 48-53.

[11] Klimontovich, Y. L., "Kinetic Equations for a Classical Nonideal Plasma," *Soviet Physics, Journal of Experimental and Theoretical Physics*, Vol. 35, 1972, pp. 920-925.

[12] Spitzer, L., *Physics of Fully Ionized Gases*, Interscience Publishers, Inc., New York, 1956, pp. 77-83.

[13] Dupre, J., *Theorie Mechanique de la Chaleur*, Masson & Cie, Paris, 1869, pp. 1-60.

[14] Buckingham, E., "Similar Systems and Dimensional Equations," *Physical Review*, Vol. 4, 1914, pp. 345-376.

[15] Buneman, O., "Dissipation of Currents in Ionized Media," *Physical Review*, Vol. 115, 1959, pp. 503-517.

[16] Hamberger, S. M., and Friedman, M., "Electrical Conductivity of Highly Turbulent Plasma," *Physical Review Letters*, Vol. 21, 1968, pp. 674-677.

[17] Sommerfeld, A., and Bethe, H., "Electron Theory of Metals," *Handbook of Physics*, Vol. 24/2, Springer Verlag, Berlin, 1933, pp. 499-536.

AIAA 81-4095

Longitudinal Grooves for Bluff Body Drag Reduction

B. Quass,* F. Howard,† L. Weinstein,* and D. Bushnell‡

NASA Langley Research Center, Hampton, Va.

Nomenclature

C_D = aerodynamic drag coefficient based on maximum cross-sectional area

D = body diameter, 6.081 cm

R = planform fairing radius at cylinder-cone junction

$R_{\infty,D}$ = freestream Reynolds number based on body diameter

Received July 11, 1980. This paper is declared a work of the U.S. Government and therefore is in the public domain.

*Aerospace Engineer, Fluid Mechanics Branch, High-Speed Aerodynamics Division. Member AIAA.

†Aerospace Engineer, Fluid Mechanics Branch, High-Speed Aerodynamics Division.

‡Head, Fluid Mechanics Branch, High-Speed Aerodynamics Division. Associate Fellow AIAA.

THE worsening world oil supply situation has placed increased emphasis upon drag reduction approaches for all forms of transportation. While aircraft cruise drag is composed primarily of skin friction and drag due to lift, the automobile (and upswept military aircraft fuselage) drag problem is still one of flow separation control (reduction of form or pressure drag). Estimates in Ref. 1 indicate that a 40% reduction in automobile aerodynamic drag would result in an increase in fuel economy the order of 16%. Typically, automobiles (along with bullets, bombs, and some planetary entry shapes) are low fineness ratio (order of 3) bluff bodies. It is possible, by moving the maximum thickness far forward and using a gradual afterbody closure, to eliminate most flow separation and thereby obtain low drag coefficients even for such low fineness ratios. However, this approach typically does not provide sufficient volume for passengers, cargo, and motive power. Therefore, ground transportation bodies are typically truncated, rather sharply, resulting in large form drag.

Several techniques are available for reducing such bluff body drag in the two-dimensional case (see Ref. 2 and references therein). However, two-dimensional techniques are not generally successful in the axisymmetric or fully three-dimensional base separation case,[3] e.g., it has generally proven much more difficult to reduce base drag in three-dimensional situations. Boattailing (gradual afterbody closure), mass addition, and base cavities are the usual techniques quoted as applicable to three-dimensional flows.[3] It should be noted that there has not yet been a systematic application of the myriad diffuser separation control techniques (e.g., Ref. 4) to the bluff body separation problem (which could be looked upon in some sense as an inside-out diffuser). The present Note describes recent bluff body drag tests involving the use of large scale longitudinal surface grooves.

The axisymmetric configurations employed in the present study are indicated on Fig. 1. The high fineness ratio body (model A) was used as an end-point check, due to the presence of primarily attached flow in the base region. Model B was the basic separated afterbody flow configuration while model C consisted of only the forebody section of model B and was tested as a crude check on the Kammback closure concept; this concept being that the afterbody downstream of separation generally does not appreciably influence the base pressure/drag level. Model D is a grooved model for determining whether such grooves might possibly yield a base drag reduction. No attempt was made in this study to optimize either groove geometry or location.

The experiments were conducted in the Langley 7×11 in. low speed flow channel[5] with the models mounted from their side on a thin strut which was attached to a nulling, 4-point suspension drag balance.[5] These models were originally designed for a larger facility and therefore there is a blockage error of the order of 10% (from method of Ref. 6) in the present results. The actual drag would be lower than the data quoted herein. However, this correction should be the same order for all the low fineness models tested and therefore differences in results between the configurations should still be meaningful. Smoke wire flow visualization data were also obtained, as a guide to the determination of separated flow presence and boundary-layer transition regions. Figure 2 presents typical smoke wire results while Fig. 3 summarizes the drag coefficient data at zero yaw.

The visualization and drag data indicate that the flow on model A is primarily attached, with transition occurring downstream of the afterbody shoulder, i.e., in the adverse pressure gradient region (the freestream turbulence level in

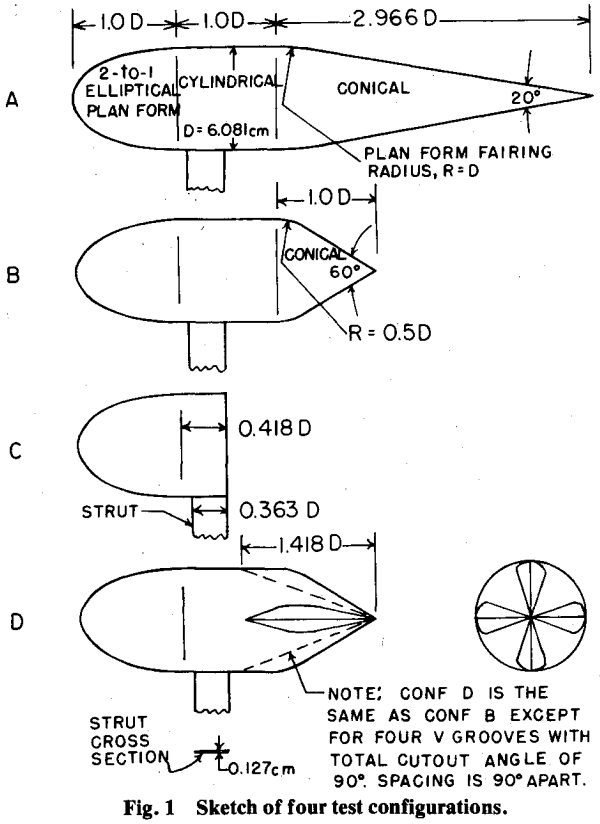

Fig. 1 Sketch of four test configurations.

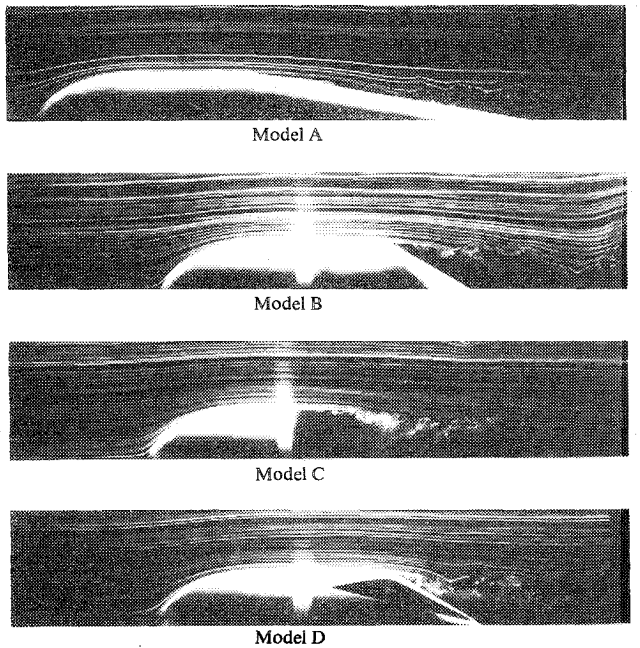

Fig. 2 Smoke wire flow visualization, $R_{\infty,D} \approx 0.8 \times 10^5$.

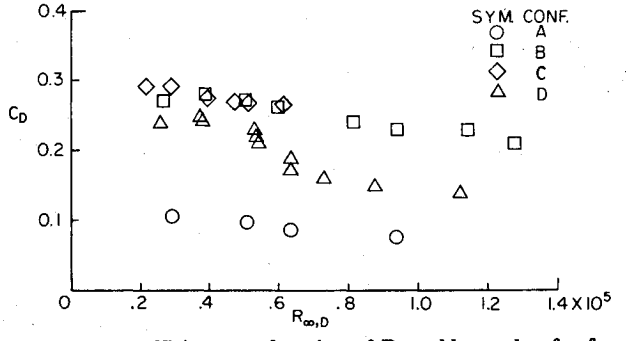

Fig. 3 Drag coefficient as a function of Reynolds number for four configurations.

this facility is the order of 0.2%). The results for model B indicate separation occurring at the shoulder and attendant higher drag levels. As expected, the drag coefficients of models B and C are quite close. Transition seems to occur in the separated shear layer and there is no apparent evidence of large scale vortex shedding.

The grooved body results are quite encouraging. The drag, for the higher Reynolds numbers, is reduced by the order of 40% and the visualization indicates the separated shear layer closure angle has moved approximately halfway toward the body. The model was tested with the grooves rotated 45 deg in the azimuthal direction from their position shown in Fig. 1. The obvious question concerning these grooved body data is "what mechanism is responsible for the drag reduction?" The original intent was that the grooves should serve simply as large scale (and continuous) longitudinal vortex generators. Extrapolation of diffuser experience with conventional vortex generators (which are usually contained within the boundary layer and of limited streamwise extent) indicated that the present 30 deg afterbody closure required a treatment considerably stronger than they could provide. A possible contributor to the present favorable results could be disruption of the shear layer instability waves ("coherent structure") by groove induced azimuthal flow variations.[7-9] Further research is required to elucidate the physical basis for the present results and optimize the effect.

References

[1] "Vehicle Aerodynamics: The Next Fuel Economy Frontier," *Automotive Engineering*, Vol. 86, July 1978, pp. 19-24.

[2] Hefner, J. N. and Bushnell, D. M., "An Overview of Concepts for Aircraft Drag Reduction," AGARD Rept. 654, 1977, pp. 1-1 - 1-30.

[3] Mair, W. A., "Drag-Reducing Techniques for Axi-Symmetric Bluff Bodies," *Aerodynamic Drag Mechanisms of Bluff Bodies and Road Vehicles*, Plenum Press, New York, 1978, pp. 161-187.

[4] Chang, P. K., *Control of Flow Separation*, Hemisphere Publishing Corp., McGraw-Hill Book Co., New York, 1976.

[5] Hefner, J. N. and Weinstein, L. M., "Re-Examination of Compliant Wall Experiments with Air with Water Substrates," *Journal of Spacecraft and Rockets*, Vol. 13, Aug. 1976, pp. 502-503.

[6] Sykes, D. M., "Blockage Corrections for Large Bluff Bodies in Wind Tunnels," *Advances in Road Vehicle Aerodynamics 1973*, edited by H. S. Stephens, BHRA Fluid Engineering, pp. 311-322.

[7] Kuethe, A. M., "Effect of Streamwise Vortices on Wake Properties Associated with Sound Generation," *Journal of Aircraft*, Vol. 9, Oct. 1972, pp. 715-719.

[8] Pannu, S. S. and Johannesen, N. H., "The Structure of Jets from Notched Nozzles," *Journal of Fluid Mechanics*, Vol. 74, Pt. 3, 1976, pp. 515-528.

[9] Bradbury, L.J.S. and Khadem, A. H., "The Distortion of a Jet by Tabs," *Journal of Fluid Mechanics*, Vol. 70, Pt. 4, 1975, pp. 801-813.

AIAA 81-4096

Stress Intensity Factors in a Biaxial Stress Field

A.F. Liu*

Northrop Corporation, Hawthorne, Calif.

IT has been discussed [1,2] that lateral tension or compression stresses would not affect the elastic stress intensity factors for a central straight crack in a plate. However, if a crack (or cracks) comes out of a circular hole in a plate, compressive loading parallel to the crack can cause tensile mode 1 stress intensity factors. On the other hand, tensile stresses parallel to the crack reduce the stress concentrations at the hole and thus reduce the crack tip stress intensity factor. Bowie's solutions[3] have provided stress intensity factors for a single crack (or cracks) emanating from the edge of a circular hole, in an infinitely wide plate, under uniaxial and the one-to-one biaxial loading conditions. For any other biaxial load ratios (either tension combined with tension or tension combined with compression), stress intensity factors can be developed by using superpositions of the uniaxial and biaxial solutions of Bowie as illustrated in Fig. 1. Following this superposition logic, stress intensity for any biaxial loading combinations can be expressed as:

$$K=[(\sigma_y-\sigma_x)B_0+\sigma_x B_1]\sqrt{\pi a} \tag{1}$$

where B_0 is the Bowie factor for uniaxial loading and B_1 is the Bowie factor for one-to-one biaxial loading; a is the crack length on either side of the hole; σ_y is the far-field gross area stress perpendicular to the crack (always in tension), and σ_x is the far-field gross area stress parallel to the crack (either in tension or compression). Let $B=\sigma_x/\sigma_y$, Eq. (1) can be written as,

$$K=\sigma_y\sqrt{\pi a}[(1-B)B_0+B\cdot B_1] \tag{2}$$

and the sign for B may be either (+) or(−).

If the hole is inside a finite width plate, the plate dimensions influence the stress concentration at the edge of the hole and thereby vary the stress intensity factor. Furthermore, finite width dimension also increases the crack tip stress intensity as if the hole was never there. Modifications to Eq. (2) have been reported in the literature (see Refs. 4 and 5 for $B=0$). For engineering purposes, Eq. (2) can be written as,

$$K=\sigma_y\sqrt{\pi a}[(1-B)B_0+B\cdot B_1]\cdot F \tag{3}$$

where F is a geometric factor accounting for the boundary effect of the specimen (e.g., width).

In a previous work of the author[6] the validity of using the compounded geometric factor was examined. The cases studied were double cracks at a hole in a specimen subjected to remote uniaxial cyclic loading. Constant amplitude crack growth rate data were obtained from specimens (made of 2024-T851 aluminum) that contained various hole radius to width ratios and a wide range of crack length-to-hole radius ratios. These data points were reduced to da/dN vs ΔK format using Eq. (3), and then compared to the material baseline da/dN curves developed from center cracked specimens of which the K-solution was known. Good correlations had been obtained.

In this investigation, eight cruciform specimens of the 7075-T7351 aluminum alloy had been tested under biaxial cyclic stresses. The geometry and dimensions of the cruciform specimens were the same as those reported in Ref. 2 but contained a circular hole of 6.35 mm, or 19.05 mm, in

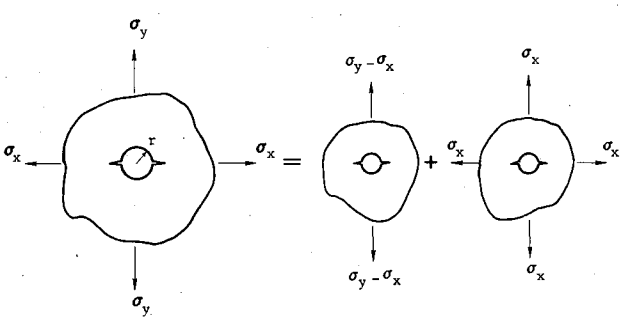

Fig. 1 Evaluation of Bowie's factor for biaxial loading.

Received Sept. 2, 1980.

*Senior Technical Specialist, Structures Life Assurance Research, Aircraft Division.